INFLUENCES OF CELL SIZE, CELL WALL THICKNESS AND CELL CIRCULARITY ON THE COMPRESSIVE RESPONSES OF CLOSED-CELL ALUMINUM FOAM AND ITS FEA ANALYSIS

Karan Singh Verma and **Dilip Muchhala**
Academy of Scientific and Innovative Research (AcSIR), Ghaziabad 201002, India

Sanjay Kumar Panthi and D. P. Mondal
CSIR-Advanced Materials and Processes Research Institute, Bhopal 462026, India

Abstract

In this study, the consequence of cell-size, cell-wall-thickness and cell circularity together on the compressive performance of closed-cell aluminum foam was analyzed experimentally and with FEM simultaneously. The closed-cell metal foams (CAFs) with varying cell sizes of 55% porosity were synthesized through stir casting technique. The granular metallic calcium is used as a stabilizing/thickening agent, and TiH$_2$ powder used as a foaming agent. The uniaxial compression tests were performed to investigate the compressive deformation behavior of CAFs. The simulation studies were carried out by taking the assumption similar to experimental constraints. The circular-shaped cells were created in FE half symmetrical model of varying cell sizes (in 2-Dimensional). The cell sizes used in FE models are 1.5 mm, 2.5 mm, 2.8 mm and of 3.5 mm. While in experimental samples, different cell sizes obtained are 1.65 mm, 2.47 mm, 2.88 mm and 3.59 mm. In both of the investigations, it is observed that the energy absorption capacity and plateau strength decrease with an increase in cell sizes or vice versa. A similar effect was also observed with an increase in cell wall thickness. The obtained FE results are acceptable and comparable with the experimental for each cell size model. The deformation mechanism was analyzed using deformed sample images, which were captured during the deformation as well as during the different stages in the FEA models.

Keywords: *porous material, finite element analysis, simulation, deformation structure*

Introduction

Aluminum foams are lightweight, porous materials in which the aluminum matrix are separated by gas-filled pores. Due to the presence of these gas-filled pores, the specific properties (strength to weight ratio) of aluminum foam are very high compared to dense aluminum. The exceptional combination of physical and mechanical properties makes aluminum foams useful in various engineering applications, such as the automotive and aircraft industry.[1,2] Commonly, metal foams are classified based on their cell morphology and based on that, metal foam can be categorized into two main groups known as closed-cell foam and open-cell foam.[3] In closed-cell metal foams, the cells are isolated by cell walls. Whereas in open-cell foam, the cells are interconnected with each other by its cell edges only.[4] Day by day, the researcher's inclination toward the fabrication of closed-cell aluminum alloy foams are increased, and many advanced fabrication techniques were developed. This may be due to lightweight, the combination of exceptional structural properties and lower fabrication temperature.[5–10] The shock absorption capacity of aluminum alloy foams is comparatively higher than the parent material due to extended plastic deformation behavior.[11,12] Therefore, aluminum alloy foams can be employed as a shock absorber in the automobile and aerospace industry. It can absorb a substantial amount of energy at very low stress during an accident that transfers the minimum shock to the passenger and mitigates the chance of injury.[13–20] Although numerous fabrication and

characterization investigations have been reported, the aluminum foams still are imperfectly characterized.[21,22] It is required to investigate metal foams in more detail with different parameters. It is observed that there are many other parameters apart from the porosity or relative density that affects the compressive behavior of foam. Gao et al.[23] worked to understand the change in aluminum properties concerning repeated impacts. This study observed that with increase in the quantity of impacts, enhanced energy absorption elastic limits stress, transmission rate, degree of damage and the respective strain. It was discovered previously that cell shape, cell size, materials composition, production technique, and foaming agents might affect the compressive behavior of CAFs.[24–34] Binesh et al.[35] found that the cell arrangement has an important role in the compressive behavior of aluminum foam. In this work, they have used a hollow ceramic sphere for the production of metal foam. The proper distribution of cells has an important role in the properties and behavior of aluminum foam. The previous investigations are not a clear clue about the direct or inverse result of cell sizes (CS) on the compressive performance of meta foams. In the different studies, there is different observations such as higher strength reported with an increase in cell size, strength rises with a decline in cell size or mid-size cell gives maximum strength of MF.[24,36,37] Recently, Nammi et al.[38] examined the cell-size effect on the energy absorption (E_{ab}) capabilities of AFs using the finite element method. For the numerical analysis, they developed the micro-mechanical model along with repetitive unit cells (i.e., small, medium and large sizes) of the 'tetrakaidecahedron' structure. The stress-strain response of the FE model shows three different regions of deformations; linear-elastic, constant plateau and densification reign, which represent the mimicking of actual aluminum foam. They reported that the smaller cell-size foam exhibits greater capability energy absorption. This may be happening owing to the fact that the closed foam was having a more consistently scattered system of small size cells that resist the movement of rigid walls. In addition to cell size and cell shape cell, circularity is also an important parameter that may affect deformation behavior. Y. An et al.[39] introduced a dimensionless term circularity shape factor to mathematically express the cell circularity. But, till today, there is no work reported in which the cell circularity cell size, cell and wall thickness are studied together. In previous investigations, the usefulness of TiH2 was explained, and it has been studied that the cell sizes can be controlled by using TiH2 as the foaming agent. Ghaleh et al.[40] synthesized closed aluminum foam of cell sizes ranging between 1.5 and 3.1 mm by adding 2.5 to 3.5 wt% of CaCO3 as the foaming agent. These researchers tried to establish the correlation between porosity, cell size mixing and holding time. They reported that the optimum foaming is achieved at a mixing time of 4 minutes and a holding time of 10 minutes. Kahani et al.[41] investigated that the quantity of TiH2, holding time and holding temperature affect the pores' sizes and distribution.

Yang et al.[42] have analyzed the mechanism of pores; they studied the effects of cooling and viscosity parameter on the foaming. TiH2 was chosen in this work to produce the desire pores sizes. In another work, the researchers reported positive results for casting aluminum foam of different pore sizes.[43] Sasikumar et al.[44] explained that the aluminum powder itself could be used for foaming aluminum. It was interestingly reported that additionally, there is no requirement for thickening agent and bubble stabilizer.Al powder was also used with TiH2, and better results were obtained. In the current effort, the authors endeavored to synthesize closed-cell aluminum alloy foam through the direct foaming (stir casting) method using titanium hydride as a foaming agent. In the present study, oxidized titanium hydride (TiH_2) powder was used as a foaming agent due to its higher specific hydrogen content, and its dissociation temperature (450 °C) is considerably closer to the melting point (i.e., 570 °C) of the alloy. Some researchers reported that the dissociation temperature of TiH_2 could be further increased when it is oxidized at the temperature of 450 °C.[45,46] The differential scanning calorimetry (DSC) studies of TiH_2 at various temperatures show the rapid dissociation kinetic, and it evident as a sharp peak in the DSC results. Although, the TiH_2 powder has some disadvantages because it is high cost and due to lower dissociation temperature (un-oxidized conditions) compared to other foaming agents, e.g., such as CaH_2, $CaCO_3$ and ZrH_2. The importance of cell size, circularity shape factor cell and wall thickness on the deformation responses was also calculated. The various cell sizes samples prepared for experimental investigation and approximately similar relative density ($\rho_{rd} = 0.45$) FE models are developed to undertand the deformation behavior.

Materials and Method

Synthesis and Characterization of CAFs

In the current study, Al-Si alloy (i.e., LM-13) used for the synthesis of foam. The LM-13 is commonly specified as EN 1706 AC-48000 (Al–Si12CulMg1), which is similar to AA 336/339 alloys. The alloy foam can be used in the automobile and defense industries for crashworthiness applications. Metal foams have a wide range of application due to their porous structures and high specific properties. The probable application of metal foams is sandwich panels, partition walls, foam-filled structures, crashworthiness/shock mitigation in automobiles and sound absorption. Generally, the application of metal foams depends on the kind of foams matrix, cell structure (open/closed porosity) and the different density of the foam. LM-13 alloy is a heat treatable casting alloy, In the present study, LM-13 alloy was selected as a matrix material due to its excellent casting characteristics, wear resistance and high mechanical properties. The casting properties such as excellent heat crack resistance and

excellent workability (casting condition) make them attractive for foam synthesis. In the LM-13 alloy, the major alloying element 'Si' reduces the thermal expansion coefficient increases corrosion and wear resistance, and improves casting and machining characteristics of the alloy. Whereas, the minor alloying elements; Fe, Mg, Cu, Mn, Ni and Zn. The 'Fe' can be tolerated up to a level of 1.5–2.0, and it can modify the 'Si' phase by inducing several Al–Fe–Si phases, and it is often used to prevent die sticking in die-casting. The chemical composition of Al–Si12CulMg1 alloy was determined by the optical emission spectrometry (Model: SPECTRO MAX LMF05, Germany) as given in Table 1. Firstly, an ingot of Al–Si12CulMg1 aluminum alloy was cut into small pieces, and these pieces were properly cleaned by using acetone (Figure 1). Cleaned pieces (charge) kept in a straight cylindrical mold of 150-mm-diameter and 600-mm-height and was coated by the graphite. The mold was kept in an electric resistance furnace for the melting of alloy pieces. The temperature of the electric resistance furnace was maintained at 700 °C. After the melting of the alloy, the mechanical stirring was done for 2 minutes in order to ensure uniform melt temperature. After that, 1 wt% of metallic 'Ca' (with a granularity of 30 μm) was added into the melt, and simultaneously stirring was performed. The granular 'Ca' increased viscosity due to the formation of calcium oxide, calcium aluminum oxide or Al4Ca intermetallics and provided stability during foaming.[7] Then, 1 wt. % of TiH$_2$ (heat-treated at 450 °C, with the granularity of 20±5 μm) powder was added in the melt and simultaneously mixed (for 2–3 minutes) using a mechanical stirrer at 750RPM. Above 400 °C, TiH$_2$ dissociates in Ti and H$_2$ gas, which is responsible for the rise in the melt's viscosity and creation of foam, respectively. After the appropriate amount of foaming, the mold was kept outside the furnace using a mechanical crane. The mold was placed on the copper plate in order to increase the conductivity of the bottom surface, and rapid cooling was done with the help of atomized water spray. Due to this rapid cooling, hydrogen gas entrapped in the melt and formed the closed pores. After the solidification of foam, the foam billet was extracted from the mold. Figure 1 shows the mild cylindrical steel (sheet thickness of 8 mm) mold, which can be assembled and disassembled with the help of temporary fasteners. Finally, the produced foam cut into small slices (diameter of 200 mm and a height of 50 mm) with the help of the supercut machine in mechanical workshop. For uniaxial compression testing, cubical shape with dimension 25 x 25 x 25 mm³ was cut

Table 1. Chemical Composition of LM13 Aluminum Alloy (Avg. wt%)

Si	Ni	Mg	Fe	Cu	Mn	Ti	Pb	Sn	Zn	Al
13	1.5	1.2	1.0	0.8	0.5	0.2	0.1	0.1	0.1	Remaining

using electrical discharge machining (EDM) to avoid cell damage. The relative density (RD) of the cubical foam samples was measured, and samples of RD-0.45 were selected of different cell sizes and microstructural analysis and compression test carried out for these samples. The experimental and FE simulation were performed simultaneously. Four different cell sizes are obtained for the experimental sample, i.e., 1.65 mm, 2.47 mm, 2.87 mm and 3.59 mm of cell diameter. While for FE analysis, four different cell sizes are chosen of 1.49 mm, 2.5 mm, 2.8 mm and 3.5 mm of cell diameter. The different phases present in the foam material are investigated, XRD analysis was performed using the X-ray diffraction machine (model: Rigaku Mini Flex ii). Scanning electron microscope (SEM, model: Nova Nano SEM 430) and FESEM (NOVA NANOSEM-430) were employed to see the morphology of the cells and distribution of different phases in the foam material. EDX analysis and elemental mapping were also done for the observation of elemental presentation and their distribution. Uniaxial compression tests were done at a strain rate of 0.01/s to all samples on the Universal Testing Machine (model: Instron 8801). During the compression test, pictures of the samples at the different stages of the deformation were captured to analyse the deformation behavior of the foam.

FE Simulation

For the finite element analysis of closed-cell metal foam, different FE models of different cell size are made. FEM samples are considered to be cubic in size of 25mm × 25mm × 25mm. Since the specimen was cubic, the advantage of symmetry in the analysis was considered, and half symmetric models were chosen for the analysis. Figure 2 shows the FE model of different cell sizes of 1.49 mm, 2.5 mm, 2.8 mm and 3.5 mm. These models are made and analyzed with ABAQUS Simulation software. For all models, similar methods of FE are used.[47] The model is considered to be deformable, and two rigid bodies are assembled with the model for compression of the sample. Three different parts are created in the part module, one is deformable, and the other two parts are rigid bodies. Available properties of Al-Si12CulMg1 aluminum alloy are assigned to the deformable part, as shown in Table 2. In the assembly module, the part is assembled in such a way that one rigid body should be on the top, and others will be at the bottom side of the deformable body. The constraints and interactions are applied to this assembly, assuming similar to the physical experimentation condition. The dynamic explicit step has chosen for the analysis, and step time is defined. After the defining, the step timing, contacts (interactions) are defined in this surface to surface interaction, it is assigned to the surfaces that are contacting each other, and self-contacts are assigned to the circular holes that are considered as voids. To perform the compression behavior, a fixed displacement is used in
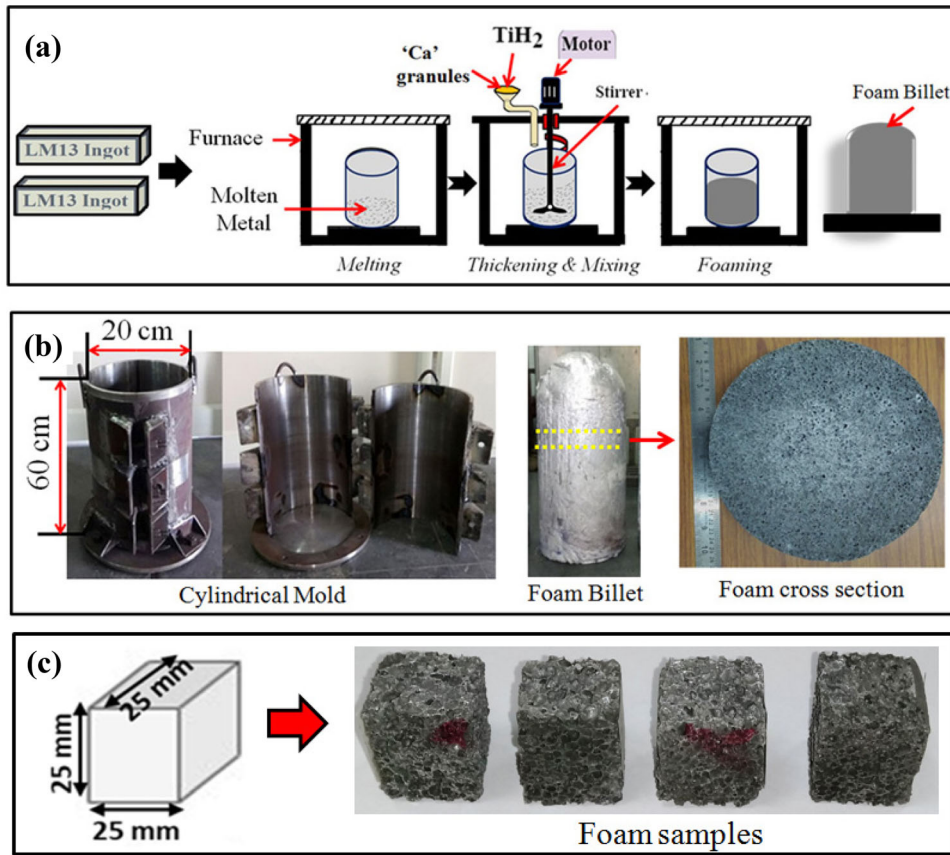
Figure 1. Schematic Diagram for the procedure of making metal foam (a) Procedure of making metal foam through stir casting techniques (b) Mold and Foam billet (c) Foam samples.
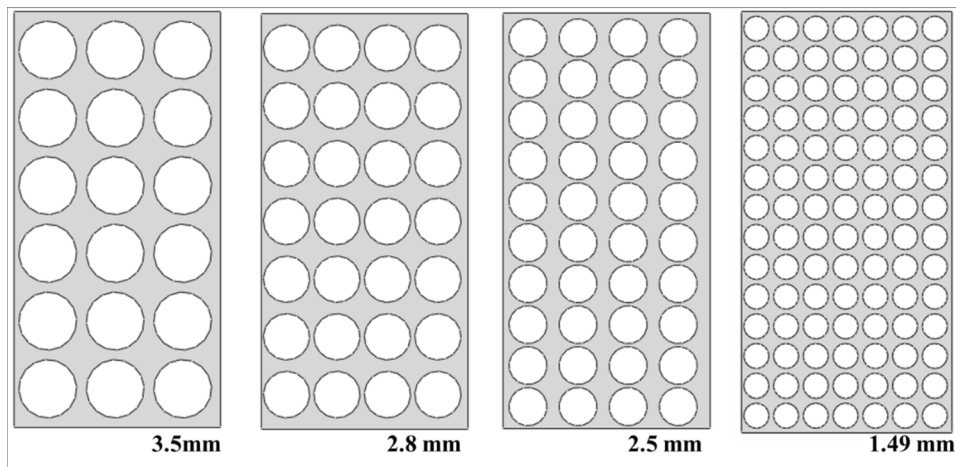

Figure 2. Different cell sizes FE models.

boundary condition that is assigned to the movable rigid body. The movable rigid bodies are mounted on the deformable part and other rigid body assigned to be fixed. The symmetric boundary condition is assigned to the vertical axis. Structural meshing is used with quadrilateral elements. After passing through these stages, the model is ready for the compressive analysis and now created job in FE software is submitted for the analysis. The calculate values of plateau strength, densification strain and energy absorption from the obtained data from ABAQUS explicit

Table 2. Material Properties of Solid LM-13 Aluminum Alloy

Plastic stress (MPa)	Plastic strain
Density- 2.6×10^{-9} ton /mm^3	
Young's modulus–69.5 GPa	
Poisson's ratio – 0.3	
203	0
222.3445	0.03338
282.3782	0.06066
308.6511	0.09304
320.3056	0.12432
325.5975	0.15719
327.8742	0.21564

solver are used for further analysis. To obtain 70% deformation of the model, distance traveled by the movable plate is set as 17.5 mm for the 25-mm-length of the model.

Material Properties

The properties of Al-Si12CulMg1 Al-alloy as given in Table 2 used in this analysis. These properties are obtained after the experimentation of a dense sample of the base metal of desire metal foam material.

Modeling

The FE models are created by the incorporation of the circular voids in the 2-Dimensional half symmetric model. The voids of equal size and in a particular pattern, these voids are arranged. For different FE model, the cell of different sizes, 1.49 mm, 2.5 mm, 2.8 mm and 3.5 mm cell diameter used.

Selection of Step Time

When the explicit solver is used for quasi-static analysis, a higher step time needs to be chosen to diminish the dynamic effect and approach the static condition. Conversely higher step time require more solution time. So optimum step time needs to be selected so that the computation time is suitable, and meanwhile dynamic effect in the simulation is insignificant. In this work, three different step time (0.0001s, 0.001s and 0.01s) are used and kinetic energy calculated for each step time. The kinetic energy calculated in Millijoule is shown for different step times, in Figure 3a showing for 0.0001s, Figure 3b showing 0.001s, Figure 3c 0.01s. Much less fluctuation was observed for the step time 0.01s. In step time 0.01s, there is tolerable fluctuation which deviates from 0.2 to 0.3 Millijoule. So for

this analysis, the step time 0.01s is chosen for further examination.

Mesh Density

It requires to study the mesh density sensitivity on the results. Finer mesh gives more accurate results than a coarser mesh. As mesh density increases the solution time is also increased, so it is required to find an acceptable element size. Model of different mesh density is used with elements size of 1554, 3295, 8547 and 12467. It was observed that with a change in the number of elements obtained results are also changed. Element size increases until the similar results are not obtained, and when it is observed that the same results are repeating this value of element size consider as optimum. In the previous publication, the stress-strain behavior for the variation in the number of an element is analysed.[48] A similar method is used for conversation study, and the change in plateau stress concerning the element size is shown in Figure 4. This analysis is carried out for 3.5 mm cell diameter FE model of 0.45 Rd. The similar procedure repeated for all of the FE models.

Results and Discussion

Morphology and Size Distribution of Cells

The cell size of AFs was measured using ImageJ software tool, and the procedure for measuring the cell size by the software is depicted in Figure 5. Firstly, the digital images (shown Figure 6) of various cell sizes were imported into the software, and after that, the image was cropped as well as it changes in the 8-bit type image. The dimension of image size is given with the help of set scale command through a known dimension. The software converts pixels of the picture into the distance which is used for further computations. Subsequently, the image adjusts the threshold (STEP-II) and then analyzes the particles size (STEP-III). And at last, the data (STEP-IV) were analyzed. Arbitrarily, 200 distinct cells were chosen for each kind of AFs, and individual cell information was collected. And, AFs cell sizes frequency distributions are presented by histogram as given in Figure 7. The calculated average cell size of AF1, AF2, AF3 and AF4 is 1.65 mm, 2.47 mm, 2.88 mm and 3.56 mm. Similarly, the average cell wall thickness for each kind of AFs was measured and listed in Table 2.

In this present study, the cell structure of aluminum foam was evaluated via a dimensionless parameter named as circularity shape factor (C_{FS}), and mathematically it can be expressed by the following relationship [25]:
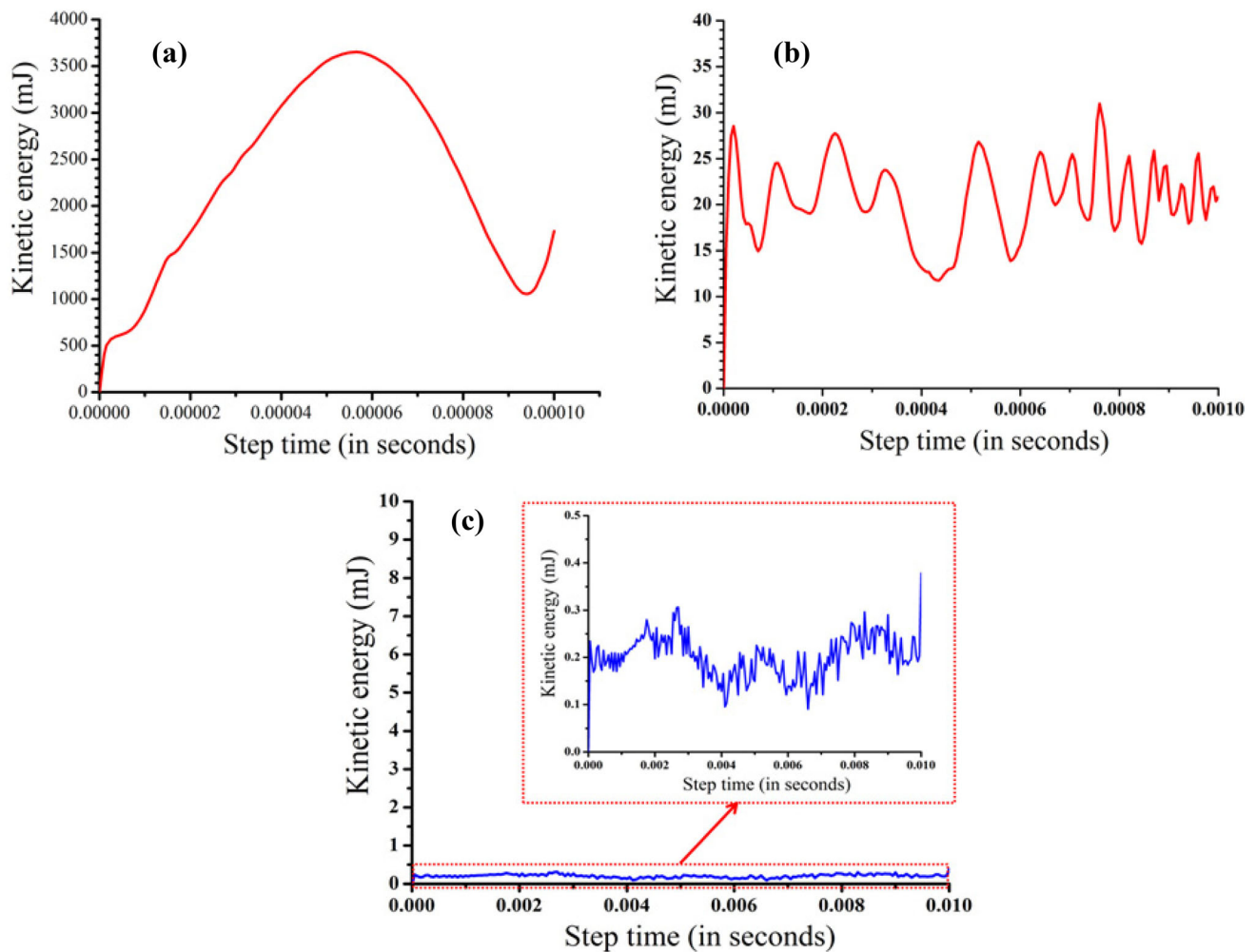
Figure 3. Presence of Kinetic energy in the model during compression with different step times (a) 0.0001s (b) 0.001s and (c) 0.01s.

$$C_{FS} = \frac{1}{N_c} \cdot \sum \frac{4\pi \cdot A_p}{P_p} \qquad \text{Eqn. 1}$$

Where N_c is the total number of cells; P_p is the perimeter and A_p is the area of the p_{th} cell respectively. The estimated values of C_{FS} was 0.855, 0.883, 0.837 and 0.813 corresponding to AF1, AF2, AF3 and AF4 respectively (Table 2).

XRD, Microstructure and EDX Analysis

X-ray diffraction patterns for the AFs samples are depicted in Figure 8 a, b separately. In these patterns, peaks of α-Al, Si and Mg2Si were detected. The peaks are similar for both samples of foam AFs. LM 13 alloy contains a small amount of Mg that reacts with Si and forms intermetallic magnesium silicide (Mg2Si). However, suppressed peaks of Mg2Si indicates its small quantity in the foam material. The microstructure of the cell wall of AF is shown in Figure 9a. The matrix of material of the cell wall of the foam is composed of two distinct phases of Al and Si. Al forms the thick dendritic structure, while silicon particles are located along the grain boundaries of the Al grains. The microstructure at higher magnification reveals that this silicon also formed the dendrites having the needle shape (Figure 9b). The elemental mapping was also performed to investigate the elemental distribution of the different elements. From the elemental mapping, it can be seen that the content of Al and Si is higher than other elements. A small amount of Mn, Mg and Ni were also detected in the elemental mapping. For more visualize image FESEM images were taken. The microstructure of foam samples was given Figure 10. From the figure, it appears that the cells are nearly spherical in shape. Figure 10a, b and c shows the
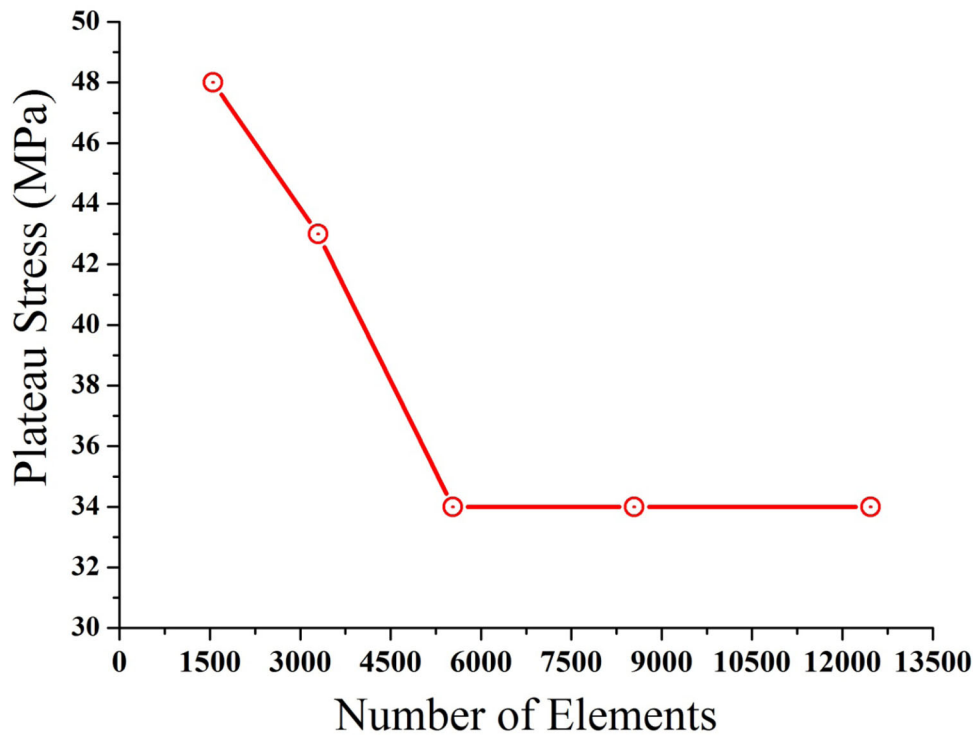
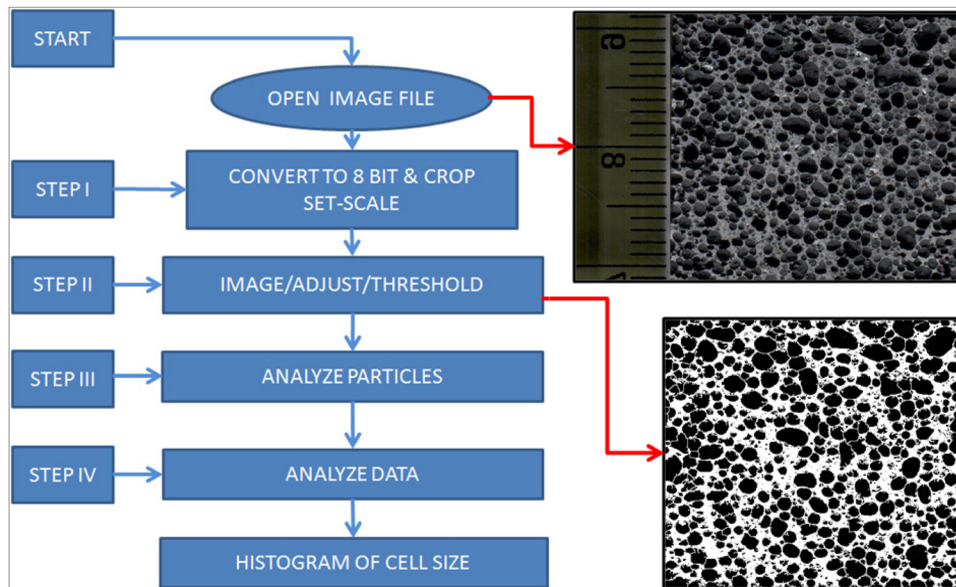**Figure 4.** *Convergence of FE results with an increase in the number of elements.*

Figure 5. *Procedure for determining the cell size of metal foam.*

microstructure of alloy foam at different magnification. In Figure 10a, the flat surface at cell wall and no presence of particles confirm the microstructure of alloy foam (also one can be observed in Figure 10b). Furthermore, it is also observed that secondary dendrites are relatively coarser in size (110-130 μm). The eutectic silicon needles and dendrites of α-Al formed during solidification on the cell walls alloy foam are easily observed in Figure 10c.

Stress-Strain Behavior

Compressive Behavior of Solid AL-SI12CULMG1 Alloy

To investigate the mechanical properties of AFs, firstly, we have to determine the properties of the matrix material. So, a dense cylindrical sample (L/d = 1.5) of Al-Si12Cu1Mg1 Al-alloy was prepared. The density of this dense sample was considered by measuring the weight and volume, and it
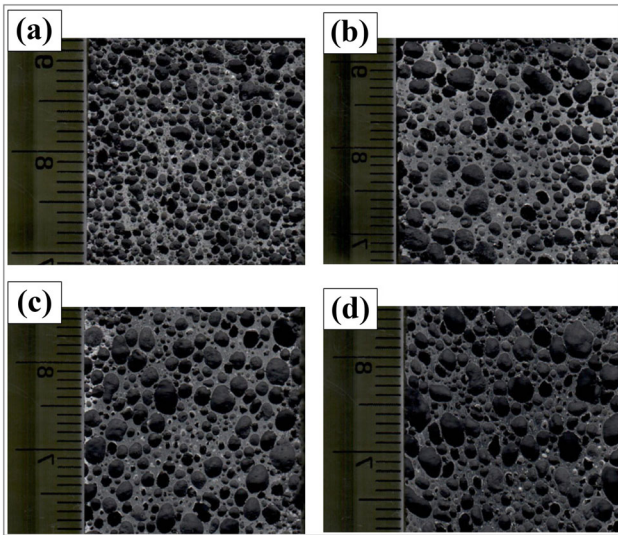
Figure 6. Different cell size samples, (a) 1.65mm (b) 2.47mm (c) 2.65mm (d) 3.59mm
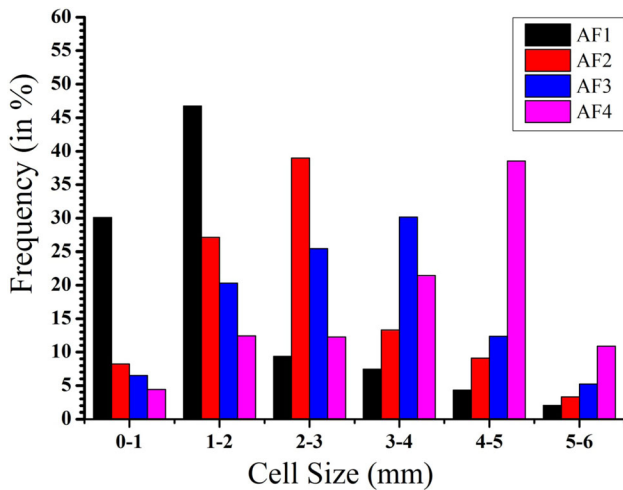

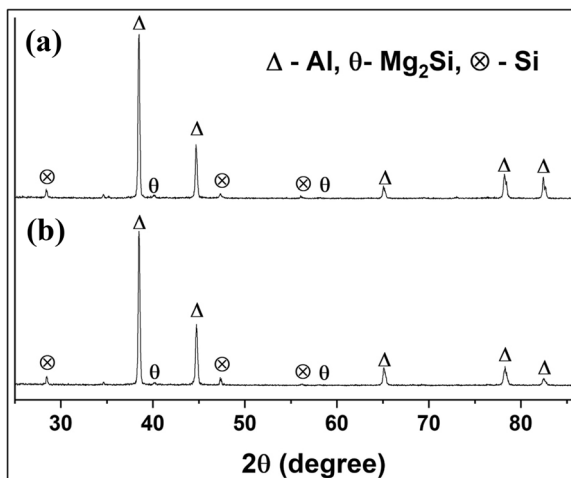**Figure 7. Cell size distribution of AFs.**
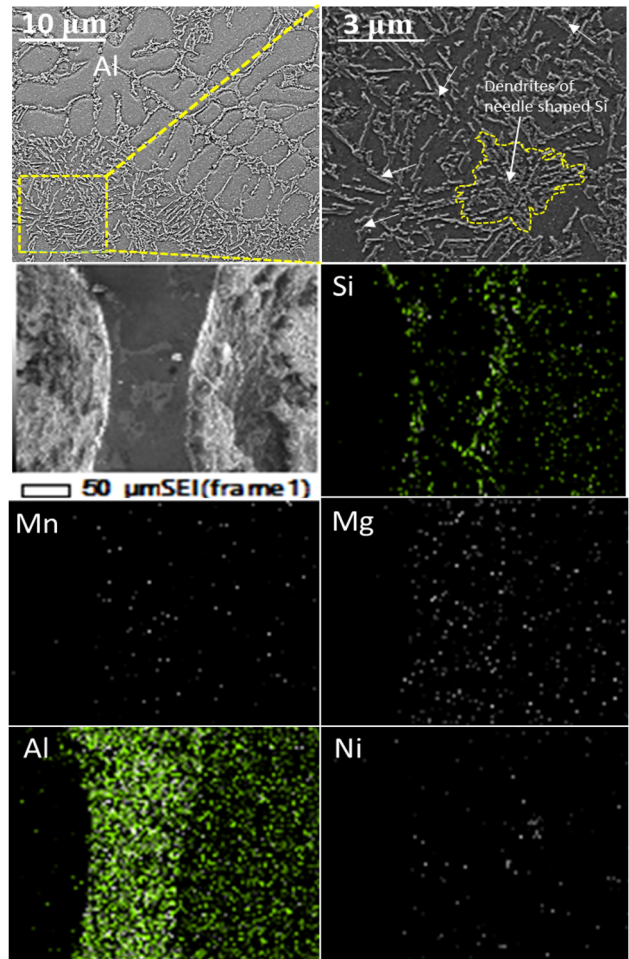

Figure 8. X-ray diffraction pattern of AFs.

Figure 9. Microstructure and EDX elemental mapping of AFs.

is found about 2.65 g/cc. The compressive stress-strain diagram of the dense sample was shown in Figure 11. The compressive proof stress (σ_{pf}) at 0.2% strain was measured 230 MP, while ultimate compressive stress (σ_{uc}) was found as 425 MPa. The strains at proof stress and failure point were observed as 0.035 and 0.26, respectively. The noted results of compressive behavior of Al-Si12CulMg1 alloy is used in simulation analysis.

Compressive Behavior of AFs

Figure 12a depicts the compressive stress-strain response of AFs. From the figure, it is observed that the stress-strain graph mainly has three different regions of deformation; (I) approximately linear-elastic region (III) nearly constant plateau region and (III) the densification region. In the linear-elastic region (I), the compressive stress and compressive strain increased approximately linear up to a maximum value of stress, i.e., plastic collapsible stress. The second deformation region (II) is the nearly constant plateau region; this region is observed between the collapsible plastic stress and the densification strain.
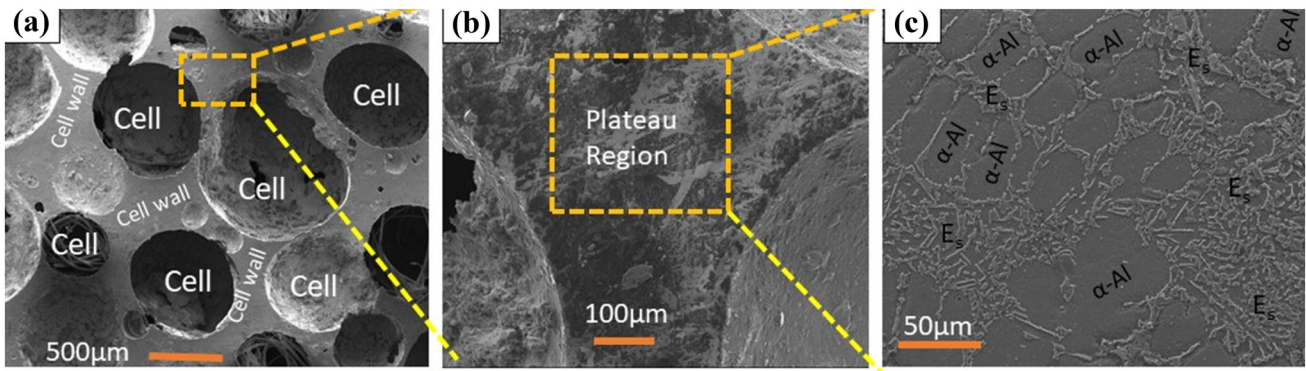
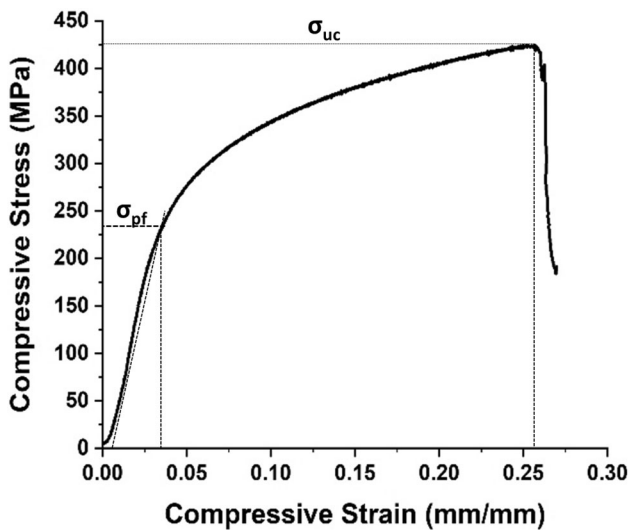**Figure 10. FESEM Image of Microstructure of Aluminum foam.**

Figure 11. Compressive Stress-Compressive strain response of LM13 alloy.

According to the ISO13314 standard, the plateau stress is termed as an average value of stresses in between strain values of 0.1 to 0.4. The densification region (III) is the last most deformation region (III) in the stress-strain graph. At the densification strain, the value of stress boosts suddenly without much increment in the strain value. The densification strain of AFs can determine with the help of tangent on the stress-strain graph (see Figure 12a). The junction point of two tangents; one is related to the plateau stress (i.e., analogous to X-axis) and second is in the densification region (for the greatest radius of curvature) of the stress-strain graph. The compressive stress-strain responses of different kind of AFs and its FEA outcomes are shown in Figure 12b, c.

Effect of Cell Size on the Deformation Behavior of AFs

Onck et al.[25] proposed a model for cellular materials to examine the result of sample size on the uniaxial compression test. According to that the plastic collapse strength (σ_{pc}) of closed-cell aluminum foams are related to the cell

size of foam and mathematically it can be represented by the following relationship:

$$\frac{\sigma_{pc}}{\sigma_{pc}^*} = \frac{\left[\left(\frac{L}{d}\right) - \frac{1}{2}\right]^2}{\left(\frac{L}{d}\right)^2} \qquad \text{Eqn. 2}$$

Where σ_{pc}^* is the plastic collapse strength of a bulk sample or sufficiently big dimension after that the effect of sample size is considerably less. *L* and *d* is the sample length and cell size of specimens, respectively. In the present investigation, the specimen length (L) is constant for various kinds of AFs, but the cell size is variable. Figure 13 shows the variation of $\frac{\sigma_{pc}}{\sigma_{pc}^*}$ with $\left(\frac{L}{d}\right)$ of AFs. From the figure, it is observed that the ratio of plastic stress of foam follow the polynomial kind of trend and the values are decreases with increase an increase in cell size. This may be due to the fraction of material present in the cell face and volume of the fraction of material exists in the cell wall, which resists the deformation of AFs. Similar trends were observed (in Table 2) for experimental and FE outcomes. The circularity shape factor is also an important factor which influences the mechanical and energy absorption properties. This may be due to that as the cell circularity increase the number of stress concentrations junctions were reduced. The cell size and cell wall thickness effects of strength of CAF are discussed in this section. The cell sizes are varied for a sample of 0.45 Rd in experimentation and FE simulation. The different cell sizes are obtained in the experimental sample are of 1.65 mm, 2.47 mm, 2.87 mm and 3.59 mm of sizes. While in FE results, the measured cell sizes are of 1.49 mm, 2.5 mm, 2.8 mm and 3.5 mm. In experimentation, the uniaxial compressive test was done on a strain rate of 0.01s, and the obtained results are plotted in the stress-strain curve, as shown in Figure 12b. From the compressive stress-strain curve, properties such as plateau strength, energy absorption, densification strain are calculated. The calculated results are tabled in Table 2. Plateau stress noted for experimental results are 35.55MPa, 32.02MPa, 28.49MPa, and 25.66 MPa for 1.65 mm, 2.47 mm, 2.87 mm and 3.59 mm cell size respectively. Also for the FE results, plateau stress is 36.93 MPa, 32.89 MPa, 30.45 MPa and 27.58 MPa
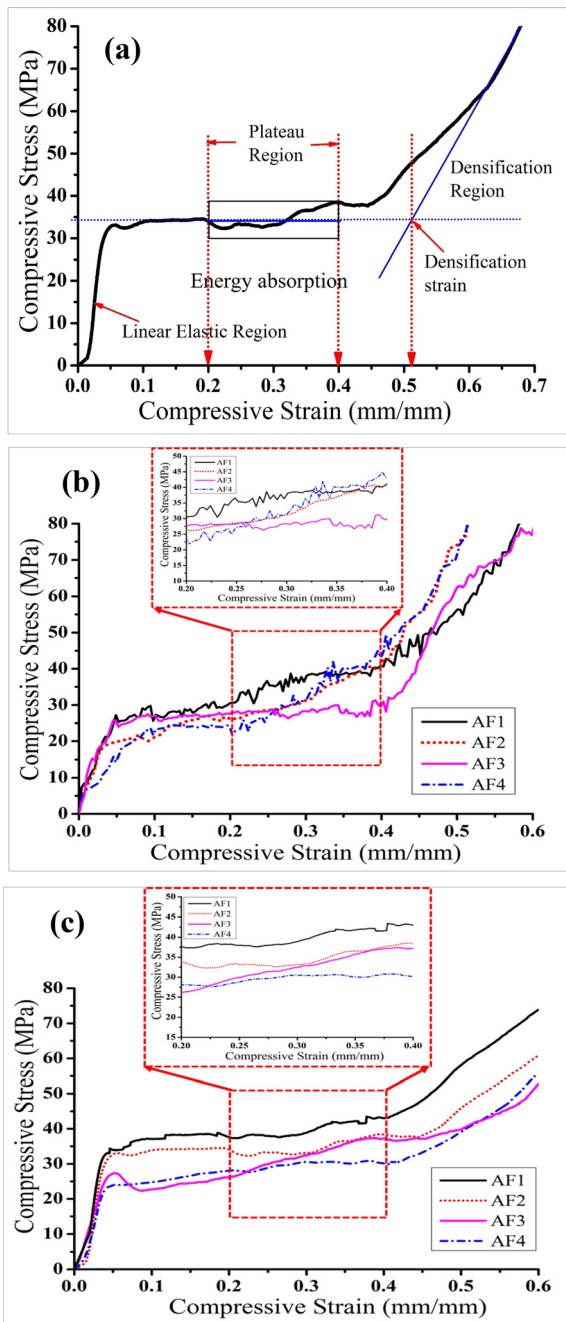
Figure 13. Variation of $\frac{\sigma_{pc}}{\sigma_{pc}^*}$ vs. cell size (d).

measured to corresponding cell size samples/models. The maximum cell thickness measured 0.568 mm and 0.571 mm for an experimental sample of 3.59 mm and FE model of 3.5 mm cell sizes, respectively. The cell wall thickness is also increased with a rise in the cell sizes, and similar behavior is reported concerning the increase in cell wall thickness on properties of AFs.

Figure 13 shows the variation of plateau stress (Experimental and FE) with cell size and circularity shape factor of different AFs. From the figure, it is found that the plateau stress decreases with an increase in cell size either in experimental or FE analysis. It is also observed that the experimental outcomes are closed to FEA outcomes. But, the difference in the experiment and FE plateau stress is minimum in case of AF2 (i.e., cell size = 2.47 mm). This may be due to the high value of circularity shape factor (i.e., 0.883). The circularity shape factor in the case of FE analysis of different AFs models is 1.0.

Energy Absorption

The energy absorption was calculated by using the area under the stress-strain curve upto densification strain. The area under the curve is calculated using the origin 8.5 software tool, and the average plateau stress is calculated as per the ISO13314 standard.[49] The calculated energy absorption values are further verified using the grid method. In this method, the grid lines were drawn on the stress-strain curve and finally count the number of grids(-covered by vertical and horizontal lines). The area of each grid was calculated, and it multiplied with the total number of grids present under the curve up to densification strain. From both the kind of method, it is found that the calculated energy absorptions are almost same

The energy absorption (E_{ab}) in case of closed-cell metal foam can be calculated using the area under the stress-

Figure 12. Compressive Stress-Strain curve (a) With different notations (b) FE results for different cell sizes and (c) Experimental outcomes of different cell sizes.

obtained for 1.49 mm, 2.5 mm, 2.8 mm and 3.5 mm cell sizes respectively. From these observations, it is noted that maximum plateau stress obtained for 1.65 mm and 1.49 mm cell size in experimental and FE results correspondingly. At the same time, the minimum plateau strength is obtained at 3.59 mm and 3.5 mm cell size of the experimental sample and FE models individually. In this investigation, it is investigated that the cell size has a significant effect on plateau strength of AFs and the strength monotonically changing with an increase or decrease in the cell sizes. Cell wall thicknesses are also
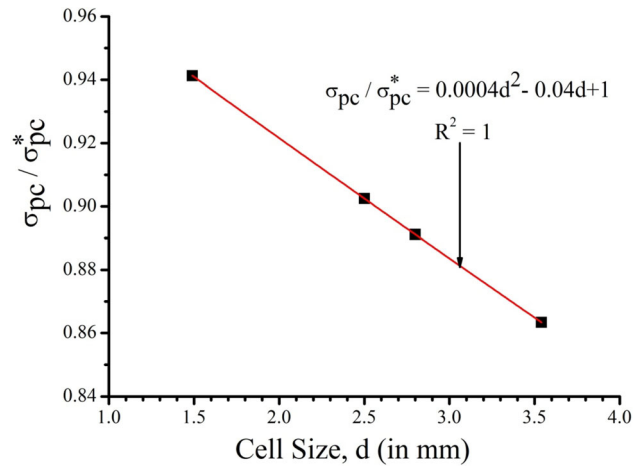
Table 3. Cell size, cell wall thickness, circularity shape factor and mechanical properties of a different kind of AFs

FEA outcomes

Foam Sign.	Cell size	Cell wall thickness	Circularity Shape factor	Plateau stress (MPa)	Densification Strain (mm/mm)	Energy absorption (MJ/m^3)
AF1	1.49	0.272	1.0	36.39	0.45	16.6185
AF2	2.50	0.403		32.67	0.41	13.4849
AF3	2.80	0.482		31.05	0.39	11.8755
AF4	3.50	0.571		28.19	0.38	10.4804

Experimental outcomes

Foam Sign.	Avg. Cell size	Avg. Cell wall thickness	Circularity Shape factor	Avg. Plateau stress (MPa)	Avg. Densification Strain (mm/mm)	Energy absorption (MJ/m^3)
AF1	1.65	0.324	0.855	34.50±2.71	0.43	14.85
AF2	2.47	0.426	0.883	31.48±1.50	0.42	13.21
AF3	2.88	0.496	0.838	28.34±2.02	0.41	11.43
AF4	3.59	0.568	0.813	25.17±1.35	0.40	10.12

strain curve, and mathematically it can be expressed by following relationship.[50,51]

$$E_{ab} = \int_0^{\varepsilon_D} \sigma_{pl}.d\varepsilon \qquad \text{Eqn. 3}$$

Where σ_{pl} and ε_D are plateau stress and densification strain of AFs, which are recorded in Table 3. It is noticed from the table the densification strain does not follow any particular trend with cell size but plateau stress decrease with an increase in cell size.

From the Table 3, it is noted that the estimated average plateau stresses in the case of FE analysis are 5–13 % higher than their respective average experimental values. In the case of experimental investigations, for each kind of cell size, four different samples were tested, and the average values are documented for further analysis. In some cases, it is observed that the experimental plateau stress is slightly higher than the FE values for the same relative density and cell size. However, the plateau stress decreases with an increase in cell size, and this trend observed in the FE as well as experimental outcomes. The variations of average plateau stress values with cell size is shown in Figure 14. From the figure, one can easily observe that the values of average plateau stress calculated experimentally are slightly lower than their FE outcomes. This may be due to the differences in the circularity shape factor, variations in the cells sizes and their distributions. In the present paper, the authors developed four different cell size models with uniform porosities. On the other hand, the experimental samples with almost the same relative density were fabricated using the stir casting technique using TiH$_2$ as the foaming agent. Due to fabrication limitations, it is very difficult to fabricate aluminum foam with uniform

porosity and definite cell distribution. So, in this present study the authors chose foam samples with nearly the same relative density, and the average cell size calculated using ImageJ software is also closed to the FE models. It is quite true that the FE models are structurally simple but their relative density is nearly equal to the experimental specimens, giving us an idea about the mechanical properties when the same foam has a uniform cell size. From this study, the authors also are trying to understand the deformation mechanism during the FE analysis and experimental compressive deformations. The plateau stress and energy absorption during the experimental compression test are not much deviated from the FE outcomes. This may be due to the differences in the deformation mechanism. In case of FE, the cells are equal in size, whereas in the case of the experimental study the foam cells have a range of variations, and due to these variations, the larger cell start collapsing first because its cell wall behaves like plastic hinges. Similarly, the inhomogeneity in the cell wall thickness is also the reason for the lesser plateau stress during the compression of experimental specimens. However, the variation in the cell size and random distributions resulted in the comparatively higher densification strain as compared to the FE models. Pandey et al.[52] studied bimodal and trimodal porosities and investigated the plateau stress and energy absorption. They reported that the different sizes of porosities and their random distribution increase the plateau stress and energy absorption. Similarly in the present study, the different cells with different sizes increase the plateau stress and energy absorption but due to their low circularity shape factors, mechanical properties may fall below the predicted properties of the same relative density foam using FE models. The variation of energy absorption with cell size is shown in Figure 15. From the
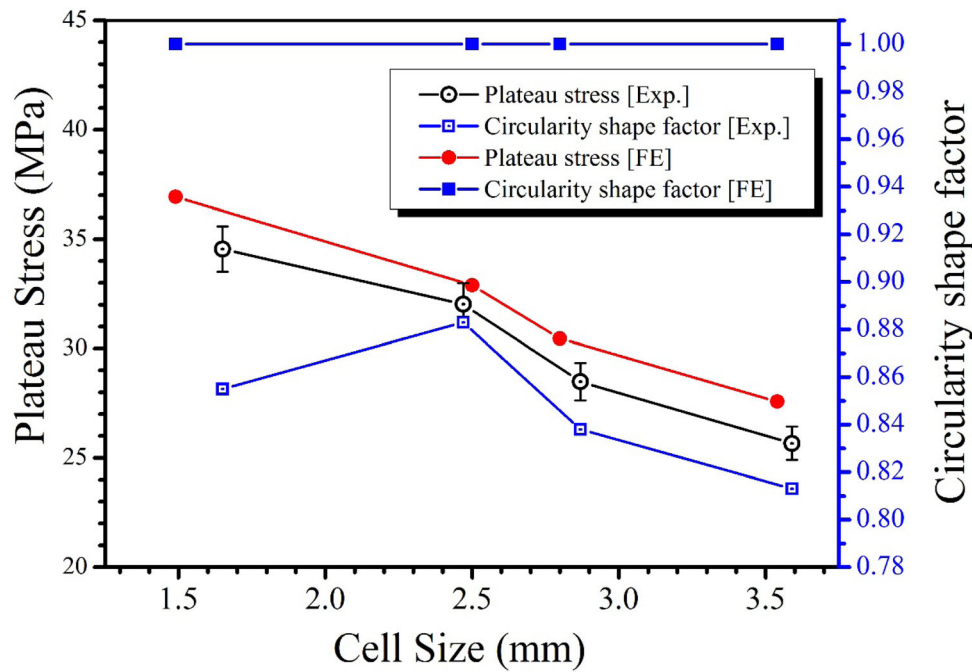
Figure 14. Variation of plateau stresses with cell sizes and circularity shape factor.
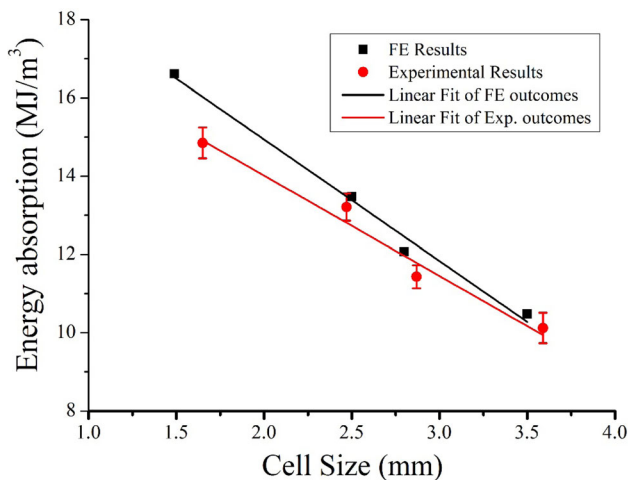

Figure 15. Variation of energy absorption with cell sizes.

figure, it is observed that the increase in cell size causes a reduction in the energy absorption capabilities of foam. This phenomenon occurs due to decrease in plateau stress and approximately similar densification strain. It is also detected the E_{ab} in case FE analysis is more than the experimental consequences. This may be a fact because of the irregularity in cell size distributions, cell shape, microstructure of matrix and portion of material existing in the cell edges.

Deformation Mechanisms

The deformation of different FE models of different cell sizes at the different strains is shown in Figure 16. As discussed and mention in Table 3, the maximum strength is observed in 1.49 mm cell size and minimum strength is seen at 2.8 cell size in FE results. This can be understood in Figure 16 that the FE model of 1.49mm cell diameter at 0.2 strain reached to maximum von Mises stress while at 2.8mm cell diameter model it did not reach to the maximum von Mises stress. So models reached to maximum von Mises stress in the different region before compressed to next stage will resist more force while a model that compressed to next stage at lower von Mises stress will resist less force. It is known that the stress is a resistive force against the external force per unit area. So the models which resist more external forces gives higher strength compared to the lesser one. In this figure, the legend shows the range of von Mises stress denoting from blue to red. Blue color shows lesser von Mises stress while red color shows higher von Mises stress, in ascending order from blue to red color. The deformation mechanism of closed-cell AFs of 0.45 relative densities with 1.65 mm cell size was investigated through its stress-strain graphs (Figure 12b) and respective images that represent the different deformation stages as shown in Figure 16 (a-d). For a better understanding of deformation, the mechanism marked cells at a different location using numbers '1', '2' '3' and '4', respectively. Figure 17a depicts the preliminary state (i.e., Figure 17a 0 %) of deformation, in which a specimen was mounted on UTM machine and then the compression test proceeded. Due to the gradual compression loading, the stretching of cell faces and bending of cell edges takes place. As a result of that linear-elastic region (I) was observed in the stress-strain graph. The bending of cell walls begins with larger cell sizes, and cells that are close to the loading surface. In this manner, the coarser cells get
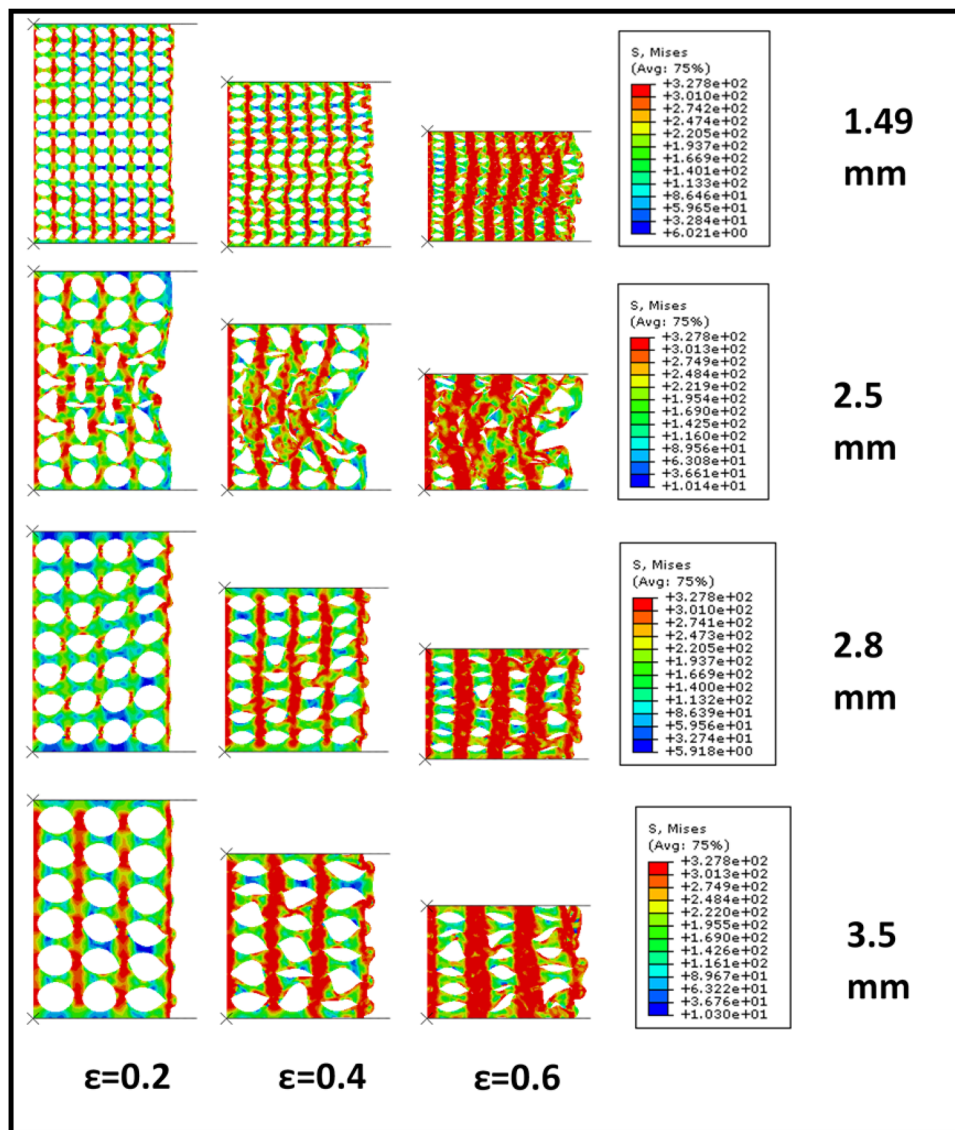
Figure 16. Deformation of different cell sizes FE models in different strains.

deformed, and cracks (marked by arrow) were initiated and propagated in the middle section of the specimen, as shown in Figure 17b. The deformation layer is on the top and bottom end of the specimen. This layer by layer (from both the ends) failure of specimen reached toward the mid-section of specimen (Figure 17c). The AFs specimen was nearly crushed (Figure 17d) and a small number of cells were present in the middle section of the specimen. It is observed that the foam cell walls during the deformation get sheared and crushed into the small flakes or debris, which is evidence that the AFs fails in a brittle way. Similar kind of deformation mechanism is observed for AF2, AF3 and AF4 irrespective of its cell sizes.

Conclusion

The metal foam can be cast into any complex shape, but cylindrical mold is used in this study. As per the common understanding, casting in more complex shapes may induce more number of casting defects in the foam due to non-uniform cooling. It required process parameters optimization according to shape as well. In future work, it can also try to fabricate foam with different complex shapes. From the above discussion, following points are concluded:

(i) AFs of 0.45 relative density with different cell sizes are successfully synthesized through stir casting technique using TiH2 as a foaming agent.

(ii) FE models of different cell sizes of 55 % porosity are fruitfully simulated, and desirable results are attained by the use of 2-Dimenstional half symmetric models.

(iii) For different cell size /cell wall thickness, different properties like E_{ab}, $\sigma_{pl,}$ and ε_D are investigated in experimentation and FE simulations.
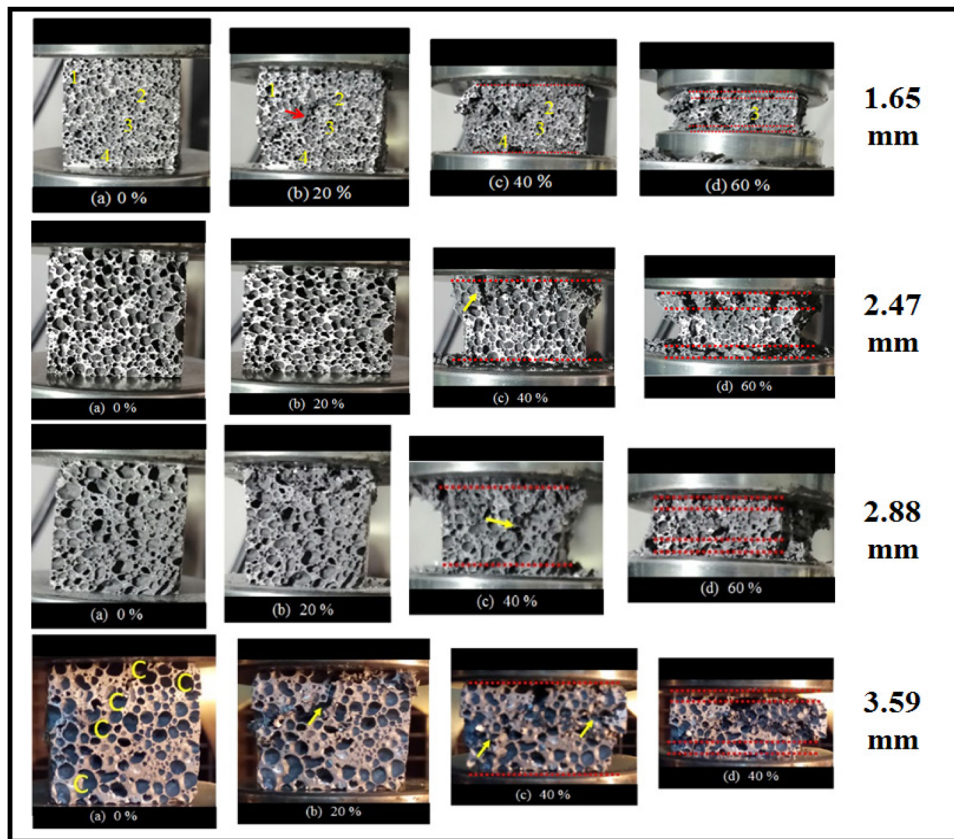
Figure 17. Different compressive stages of various cell sizes experimental samples.

(iv) Maximum plateau strength obtained by 1.49mm cell size and 1.65mm cell size in FE simulation and experimental results. While the least results are observed in the FE model of 3.5 mm and an experimental sample of 3.59 mm.

(v) Significant effects of cell size on the E_{ab} and $\sigma_{pl,}$ are noted. Better results are found for these properties by the decrease in cell sizes.

(vi) The results obtained in the FE simulation are satisfactory and comparable with the experimental results.

(vii) The circularity shape factor influences plateau strength and energy absorption of AFs. The experimental samples with the high value of circularity shape factor exhibit more close results to the FE results.

Acknowledgement

Declaration

Conflict of interest There is no conflict of interest among the authors.

REFERENCES

1. Q. Yu, Y. Zhao, A. Dong, Y. Li, Mechanical properties of EPS filled syntactic foams prepared by VARTM. Compos. Part B Eng. **136**, 126–134 (2018). https://doi.org/10.1016/j.compositesb.2017.07.053

2. V.C. Srivastava, K.L. Sahoo, Processing, stabilization and applications of metallic foams. Art of science. Mater. Sci. Pol. **25**, 733–753 (2007)

3. J. Banhart, Characterization and applications of cellular metals and metal foams. Manuf. Prog Mater. Sci. **46**, 559–632 (2001)

4. N. Fleck, Metal foams : a design guide metal foams : a design guide, 3069, 264 (2016). https://doi.org/10.1016/S0261-3069(01)00049-8

5. O.B. Olurin, N.A. Fleck, M.F. Ashby, Deformation and fracture of aluminium foams. Mater. Sci. Eng. A **291**, 136–146 (2000). https://doi.org/10.1016/S0921-5093(00)00954-0

6. Y. Wang, X. Zhai, J. Yan, W. Ying, W. Wang, Experimental, numerical and analytical studies on the aluminum foam filled energy absorption connectors under impact loading. Thin-Walled Struct. **131**, 566–576 (2018). https://doi.org/10.1016/j.tws.2018.07.056

7. R. Rajendran, K.P. Sai, B. Chandrasekar, A. Gokhale, S. Basu, Preliminary investigation of aluminium foam as an energy absorber for nuclear transportation cask.

Mater. Des. **29**, 1732–1739 (2008). https://doi.org/10.1016/j.matdes.2008.03.028

8. E.W. Andrews, G. Gioux, P.R. Onck, L.J. Gibson, F. García-Moreno, D. Schwingel, H.W. Seeliger, C. Vecchionacci, D. Alwes, J. Dittrich, C. Chen, T.J. Lu, M.D. Goel, P. Altenhofer, V.A. Matsagar, A.K. Gupta, C. Mundt, S. Marburg, R.P. Merrett, G.S. Langdon, M.D. Theobald, P.R. Onck, E.W. Andrews, L.J. Gibson, F.G. Rammerstorfer, D.H. Pahr, T. Daxner, W.K. Vonach, Aluminium foam sandwich structures for space applications. Int. J. Mech. Sci. **43**, 326–330 (2001). https://doi.org/10.1016/j.matdes.2012.08.016

9. A.G. Evans, J.W. Hutchinson, M.F. Ashby, Multifunctionality of cellular metal systems. Prog. Mater. Sci. **43**, 171–221 (1998). https://doi.org/10.1016/S0079-6425(98)00004-8

10. M.D. Goel, Deformation, energy absorption and crushing behavior of single-, double- and multi-wall foam filled square and circular tubes. Thin-Walled Struct. **90**, 1–11 (2015). https://doi.org/10.1016/j.tws.2015.01.004

11. Y. Cheng, Y. Li, X. Chen, X. Zhou, N. Wang, Compressive properties and energy absorption of aluminum foams with a wide range of relative densities. J. Mater. Eng. Perform. (2018). https://doi.org/10.1007/s11665-018-3514-4

12. D.A. Whisler, H. Kim, A. Rabiei, Author ' s Accepted manuscript high strain rate behavior of composite metal foam. Mater. Sci. Eng. A. (2015). https://doi.org/10.1016/j.msea.2015.02.027

13. M.D. Goel, V.A. Matsagar, S. Marburg, A.K. Gupta, Comparative performance of stiffened sandwich foam panels under impulsive loading. J. Perform. Constr. Facil. **27**, 540–549 (2013). https://doi.org/10.1061/(ASCE)CF.1943-5509.0000340

14. H. Zhou, Y. Wang, X. Wang, Z. Zhao, G. Ma, Energy absorption of graded foam subjected to blast: a theoretical approach. Mater. Des. **84**, 351–358 (2015). https://doi.org/10.1016/j.matdes.2015.06.124

15. J.K. Katiyar, S. Bhattacharya, V.K. Patel, V. Kumar, in *Automotive Tribology*, Energy, Environment, and Sustainability. http://www.springer.com/series/15901

16. J. Baumeister, J. Banhart, M. Weber, Aluminium foams for transport industry. Mater. Des. **18**, 217–220 (2002). https://doi.org/10.1016/s0261-3069(97)00050-2

17 R. Rajendran, K. Prem Sai, B. Chandrasekar, A. Gokhale, S. Basu, Impact energy absorption of aluminium foam fitted stainless steel tube. Mater. Des. **30**(5), 1777–1784 (2009). https://doi.org/10.1016/j.matdes.2008.07.021

18. M. Colombo, P. Martinelli, R. Zedda, A. Albertelli, N. Marino, Dynamic response and energy absorption of mineral-phenolic foam subjected to shock loading. Mater. Des. **78**, 63–73 (2015). https://doi.org/10.1016/j.matdes.2015.04.014

19. M.D. Goel, V.A. Matsagar, Blast-resistant design of structures. Pract. Period. Struct. Des. Constr. **19**, 1–9 (2014). https://doi.org/10.1061/(ASCE)SC.1943-5576.0000188

20. G. Srinath, A. Vadiraj, G. Balachandran, S.N. Sahu, A.A. Gokhale, Characteristics of aluminium metal foam for automotive applications. Trans. Indian Inst. Met. **63**, 765–772 (2010). https://doi.org/10.1007/s12666-010-0117-7

21 M.F. Ashby, A. Evans, N. a Fleck, L.J. Gibson, J.W. Hutchinson, N.G. Hayden, Book reviews. Anticancer Res **32**(1), 3594 (2012). https://doi.org/10.1016/S0261-3069(01)00049-8

22. C. Barbier, P.M. Michaud, D. Baillis, J. Randrianalisoa, A. Combescure, New laws for the tension/compression properties of Voronoi closed-cell polymer foams in relation to their microstructure. Eur. J. Mech. A/Solids **45**, 110–122 (2014). https://doi.org/10.1016/j.euromechsol.2013.12.001

23. H. Gao, C. Xiong, J. Yin, H. Deng, Research on Dynamic Accumulation effect and constitutive model of aluminum foams under dynamic impact. Int. J. Met. **13**, 146–157 (2019). https://doi.org/10.1007/s40962-018-0245-0

24 X.Q. Cao, Z.H. Wang, H.W. Ma, L.M. Zhao, G.T. Yang, Effects of cell size on compressive properties of aluminum foam. Trans. Nonferrous Met. Soc. China (English Ed) **16**, 351–356 (2006). https://doi.org/10.1016/S1003-6326(06)60060-5

25 E.W. Andrews, G. Gioux, P. Onck, L.J. Gibson, Size effects in ductile cellular solids. Part II: experimental results. Int. J. Mech. Sci. **43**(3), 701–713 (2001). https://doi.org/10.1016/S0020-7403(00)00043-6

26. R. Gradinger, F.G. Rammerstorfer, On the influence of meso-inhomogeneities on the crush worthiness of metal foams. Acta Mater. **47**, 143–148 (1998). https://doi.org/10.1016/S1359-6454(98)00332-2

27. Z. Chen, X. Wang, F. Giuliani, A. Atkinson, Microstructural characteristics and elastic modulus of porous solids. Acta Mater. **89**, 268–277 (2015). https://doi.org/10.1016/j.actamat.2015.02.014

28. P. Kenesei, C. Kádár, Z. Rajkovits, J. Lendvai, The influence of cell-size distribution on the plastic deformation in metal foams. Scr. Mater. **50**, 295–300 (2004). https://doi.org/10.1016/j.scriptamat.2003.09.046

29. T.G. Nieh, K. Higashi, J. Wadsworth, Effect of cell morphology on the compressive properties of open-cell aluminum foams. Mater. Sci. Eng. A. **283**, 105–110 (2000). https://doi.org/10.1016/S0921-5093(00)00623-7

30. J.F. Rakow, A.M. Waas, Size effects in metal foam cores for sandwich structures. 44th AIAA/ASME/ASCE/AHS/ASC Struct Struct. Dyn. Mater. Conf. **42**(7), 1331–7 (2003)

31. U. Ramamurty, A. Paul, Variability in mechanical properties of a metal foam. Acta Mater. **52**, 869–876 (2004). https://doi.org/10.1016/j.actamat.2003.10.021

32. M. De Giorgi, A. Carofalo, V. Dattoma, R. Nobile, F. Palano, Aluminium foams structural modelling. Comput. Struct. **88**, 25–35 (2010). https://doi.org/10.1016/j.compstruc.2009.06.005

33 A.H. Roohi, H. Moslemi Naeini, M. Hoseinpour Gollo, M. Soltanpour, M. Abbaszadeh, On the random based closed cell metal foam modeling and its behavior in laser forming process. Opt. Laser. Technol. **72**, 53–64 (2015). https://doi.org/10.1016/j.optlastec.2015.03.012

34. A.E. Simone, L.J. Gibson, The effects of cell face curvature and corrugations on the stiffness and strength of metallic foams. Acta Mater. **46**, 3929–3935 (1998). https://doi.org/10.1016/S1359-6454(98)00072-X

35. F. Binesh, J. Zamani, M. Ghiasvand, Ordered structure composite metal foams produced by casting. Int. J. Met. **12**, 89–96 (2018). https://doi.org/10.1007/s40962-017-0143-x

36. B. Jiang, Z. Wang, N. Zhao, Effect of pore size and relative density on the mechanical properties of open cell aluminum foams. Scr. Mater. **56**, 169–172 (2007). https://doi.org/10.1016/j.scriptamat.2006.08.070

37. C.E. Wen, Y. Yamada, K. Shimojima, Y. Chino, H. Hosokawa, M. Mabuchi, Compressibility of porous magnesium foam : dependency on porosity and pore size. Materials Letters. **58**, 357–360 (2004). https://doi.org/10.1016/S0167-577X(03)00500-7

38. S.K. Nammi, G. Edwards, H. Shirvani, Effect of cell-size on the energy absorption features of closed-cell aluminium foams. Acta Astronaut **128**, 243–250 (2016). https://doi.org/10.1016/j.actaastro.2016.06.047

39. Y. An, S. Yang, E. Zhao, Z. Wang, H. Wu, Fabrication of aluminum foam reinforced by graphene nanoflakes. Mater. Lett. **212**, 4–7 (2018). https://doi.org/10.1016/j.matlet.2017.10.043

40 M.H. Ghaleh, N. Ehsani, H.R. Baharvandi, High-porosity closed-cell aluminum foams produced by melting method without stabilizer particles. Int. J. Met. (2020). https://doi.org/10.1007/s40962-020-00528-w

41 J. Kahani Khabushan, S. Bazzaz Bonabi, F. Moghaddasi Aghbagh, A. Kahani Khabushan, A study of fabricating and compressive properties of cellular foam using. Mater. Des. **55**, 792–797 (2014). https://doi.org/10.1016/j.matdes.2013.10.022

42. C.C. Yang, H. Nakae, The effects of viscosity and cooling conditions on the foamability of aluminum alloy. J. Mater. Process. Technol. **141**, 202–206 (2003). https://doi.org/10.1016/S0924-0136(02)01048-8

43. Z.L. Song, J.S. Zhu, L.Q. Ma, D.P. He, Evolution of foamed aluminum structure in foaming process. Mater. Sci. Eng. A. **298**, 137–143 (2001). https://doi.org/10.1016/s0921-5093(00)01285-5

44 S. Sasikumar, K. Georgy, M. Mukherjee, G.S. Vinod Kumar, Foam stabilization by aluminum powder. Mater. Lett. **262**, 127142 (2020). https://doi.org/10.1016/j.matlet.2019.127142

45. F. von Zeppelin, M. Hirscher, H. Stanzick, J. Banhart, Desorption of hydrogen from blowing agents used for foaming metals. Compos. Sci. Technol. **63**, 2293–2300 (2003). https://doi.org/10.1016/S0266-3538(03)00262-8

46. B. Matijasevic-Lux, J. Banhart, S. Fiechter, O. Görke, N. Wanderka, Modification of titanium hydride for improved aluminium foam manufacture. Acta Mater. **54**, 1887–1900 (2006). https://doi.org/10.1016/j.actamat.2005.12.012

47. D.L. Logan, *A First Course in the Finite Element Method*. (2012). ISBN:9780495668251

48. K.S. Verma, S.K. Panthi, D.P. Mondal, Compressive deformation behavior of closed cell LM-13 aluminum alloy foam using finite element analysis. Mater. Today Proc. (2020). https://doi.org/10.1016/j.matpr.2020.01.081

49. I. Standard, Compression test for porous and cellular metals, Int. Stand. ISO 13314 (2011). ISO13314:2011

50. Y. Cheng, Y. Li, X. Chen, X. Zhou, N. Wang, Compressive properties and Energy absorption of aluminum foams with a wide range of relative densities. J. Mater. Eng. Perform. **27**, 4016–4024 (2018). https://doi.org/10.1007/s11665-018-3514-4

51. B.N. Yadav, D. Muchhala, P. Singh, A.N.C. Venkat, D.P. Mondal, Synergic effect of MWCNTs and SiC addition on microstructure and mechanical properties of closed-cell Al–SiC-MWCNTs HCFs. Compos. Part B **172**, 458–471 (2019). https://doi.org/10.1016/j.compositesb.2019.05.041

52. A. Pandey, S. Birla, D.P. Mondal, S. Das, V.A.N. Ch, Compressive deformation behavior and strain rate sensitivity of Al-cenosphere hybrid foam with mono-modal, bi-modal and tri-modal cenosphere size distribution. Mater. Charact. **144**, 563–574 (2018). https://doi.org/10.1016/j.matchar.2018.08.011